Fast surface measurement using wavelength scanning interferometry with compensation of environmental noise

Xiangqian Jiang,* Kaiwei Wang, Feng Gao, and Hussam Muhamedsalih

Centre for Precision Technologies, School of Computing and Engineering, University of Huddersfield, Huddersfield HD1 3DH, United Kingdom

*Corresponding author: x.jiang@hud.ac.uk

Received 12 November 2009; revised 26 March 2010; accepted 17 April 2010; posted 19 April 2010 (Doc. ID 119889); published 17 May 2010

We introduce a new optical interferometry system for fast areal surface measurement of microscale and nanoscale surfaces that are immune to environmental noise. Wavelength scanning interferometry together with an acousto-optic tunable filtering technique is used to measure surfaces with large step heights. An active servo control system serves as a phase-compensating mechanism to eliminate the effects of environmental noise. The system can be used for online or in-process measurement on a shop floor. Measurement results from two step height standard samples and a structured surface of a semiconductor daughterboard are presented. In comparison with standard step height specimens, the system achieved nanometer measurement accuracy. The measurement results of the semiconductor daughterboard, under mechanical disturbance, showed that the system can withstand environmental noise.

OCIS codes: 120.6660, 120.3180.

1. Background

In developed economies the manufacture of high added-value critical components is rapidly shifting to the design and fabrication of microstructure and nanostructure and free-form surfaces [1,2]. The market for components that possess these surfaces is huge, is growing by 25% per year (1996–2005), and is receiving significant investment worldwide [3].

The increased use of nanoscale and ultraprecision structured surfaces is wide ranging and covers optics, silicon wafers, hard disk drives, microelectromechanical systems and nanoelectromechanical systems (MEMS/NEMS), microfluidics, and micromolding industries. These industries all rely critically on ultraprecision surfaces. There is, however, a fundamental limiting factor to the manufacture of such surfaces, namely, the ability to measure the product quickly and easily within the manufacturing environment. It has been reported that currently the quality of fabrication depends largely on the experience of process engineers backed by an expensive trial-and-error approach. Consequently, many of these manufactured items suffer from scrap rates as high as 50–70% [4].

Optical interferometry has been widely explored for surface measurement because of the advantages of noncontact and high accuracy interrogation. However, conventional optical interferometry techniques are extremely sensitive to environmental noise such as mechanical vibration, air turbulence, and temperature drift. These noises cause errors in surface measurement and can produce invalid results. To overcome this problem there are a number of ways to reduce the effect of these noises. Although controlling the environment by using a vibration isolation stage and maintaining a fixed temperature is an effective way of reducing noise for laboratory and offline applications, it is not practical in a manufacturing situation, for example, when the target is too large to be mechanically isolated. Another method is to acquire

0003-6935/10/152903-07$15.00/0

the data as fast as possible by employing a high speed camera and fast phase-shifting method or even taking all the required data simultaneously [5–8]. Complete common-path interferometers such as the scatter-plate interferometer are also insensitive to noise [9–11]. These noise reduction methods are usually reserved for laser-based phase-shifting interferometry, which is limited to the measurement of relatively smooth surfaces that are due to the well-known phase ambiguity problem of monochromatic interferometry.

White-light vertical scanning interferometry can overcome the 2π phase ambiguity problem and extend the field of application of interferometric profilometry to rough surfaces and structured surfaces with large step heights [12–16]. It enables the absolute measurement of the optical path difference (OPD) by determining the peak position from the interferogram. It can be used to measure both optically smooth and rough surfaces. Optically smooth surfaces are defined as having height variations within the resolution cell of the imaging system not exceeding one-eighth of the wavelength of the light used; optically rough surfaces are defined as having height variations within the resolution cell of the imaging system exceeding one-fourth of the wavelength of the light used, although the evaluation methods of the measurement signal differ [12,15,17,18]. However, the need to perform mechanical scanning of a heavy probe head or the specimen stage limits the measurement speed. In addition, the data acquisition procedure and processing are more complicated than for monochromatic interferometry.

Wavelength scanning interferometry (WSI) using a two-dimensional CCD detector has been reported by many researchers worldwide in the field of areal surface measurement [19–26]. In comparison with white-light vertical scanning interferometry, surface topography measurements of WSI are based on the phase shifts that are due to wavelength variations, thus avoiding any scanning by mechanical movement. Absolute OPD can still be measured without any 2π phase ambiguity. WSI advanced itself to dispersive white-light interferometry [27–32] by measuring the full field of a surface instead of a single point or a profile of the surface by means of spectrometry.

We propose a fast, environmentally robust, surface measurement system using wavelength scanning interferometry and active servo control techniques. The phase and surface measurement principle is described. Measurement results from two step height standard samples and a structured surface of a semiconductor daughterboard are presented. In comparison with the standard step height specimens, the system achieved nanometer measurement accuracy. The measurement results on the semiconductor daughterboard under mechanical disturbance show that the system can withstand environmental noise. The proposed measurement system can be used in online or in-process measurement to measure and characterize free-form structured surfaces.

2. Experimental Setup

The basic configuration of the proposed surface measurement system is illustrated in Fig. 1. The measurement system is composed of two Linnik interferometers that share a common optical path. The measurement interferometer, illuminated by a white-light source, is used to acquire a three-dimensional surface of the sample. The reference interferometer, illuminated by a near-infrared superluminescent light-emitting diode (SLED), is used to monitor and compensate for the environmental noise, e.g., temperature drift, mechanical vibration,

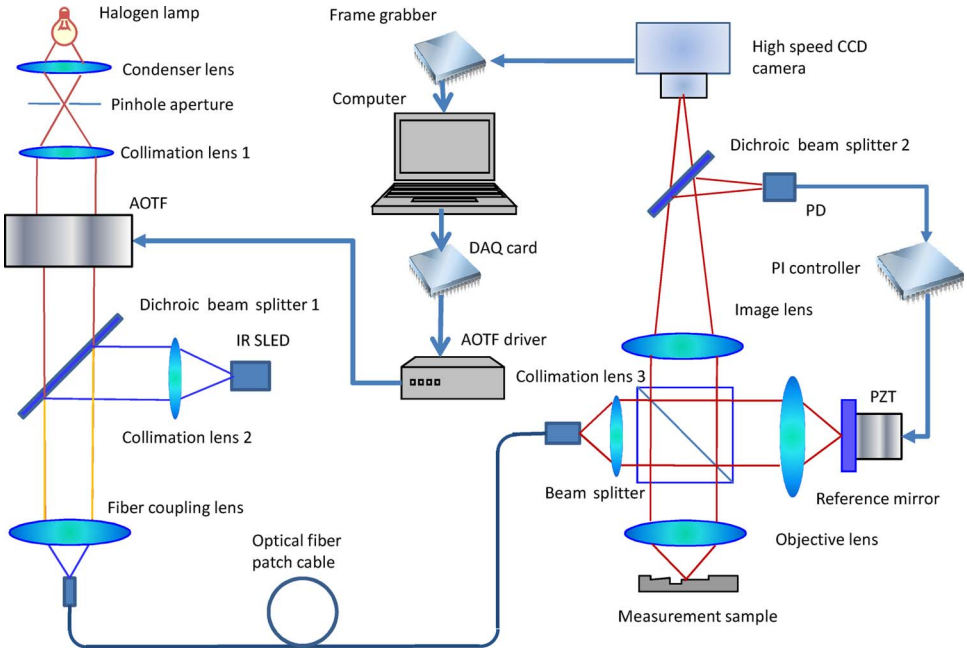

Fig. 1. (Color online) Proposed surface measurement system: PD, photodiode; DAQ, data acquisition card.

and air turbulence. As the two interferometers suffer similar environmental noise, the measurement interferometer will be capable of measuring surface information after the reference interferometer is locked into the compensation mode.

The light beams from the white light and the SLED are coupled by the dichroic beam splitter that is highly reflective at the infrared SLED wavelength and transmissive in the visible light wavelength range. After passing through the dichroic beam splitter, the light beam is coupled to an optical fiber path cable by a fiber coupling lens. The light beam is transmitted to the interferometer system and is collimated by lens 3. The system adopts a Linnik configuration that has the ability to compensate for chromatic dispersion and other optical aberrations. Light reflected by the sample and the reference mirror are combined by a beam splitter to generate an interferogram.

A key feature of this experimental setup is the acousto-optic tunable filter (AOTF), which is placed behind the white-light source to select a specific wavelength thus producing an interferogram at the CCD source only at that specific wavelength. The selected light wavelength is determined by

$$\lambda = \Delta n \alpha \frac{v_a}{f_a}, \tag{1}$$

where Δn is the birefringence of the crystal used as the diffractive material, α is a complex parameter that depends on the design of the AOTF, and v_a and f_a are the propagation velocity and frequency of the acoustic wave, respectively. The wavelength of the light that is selected by this diffraction can therefore be varied simply by changing driving frequency f_a. Different wavelengths of light pass through the AOTF in sequence so that a series of interferograms are detected by the CCD. The absolute OPD can be calculated by analyzing these interferograms.

Current AOTFs have a typical resolution of from 1 to 10 nm, which is determined by design parameters. This results in a coherence length of approximately 30–400 μm for the diffracted light. Thus no interferogram will be detected when the OPD of the measurement interferometer is larger than the coherence length. The particular AOTF in our experimental setup restricts the vertical measurement range of this technique to approximately 200 μm.

Surface measurement in a workshop and manufacturing environment has been difficult to achieve with interferometric methods because they are so sensitive to vibrations, in particular, axial (vertical) vibration [33]. In addition, measurement noise can also be induced by temperature drift and air turbulence. In this experiment, the reference interferometer is illuminated by a single wavelength laser and is employed together with a servo feedback electronic unit to effectively compensate for the environmental noise. Light output from the laser is combined with the measurement light and travels almost the same optical path as the measurement interferometer. The interference signal of the reference interferometer is acquired with a photodiode after it has been filtered by beam splitter 3. As a result of the shared optical path, it is envisioned that, if the noise that occurs in the reference interferometer is monitored and compensated for, the measurement interferometer will not observe noise during measurement. A compensating piezoelectric translator (PZT) attached to the reference mirror is driven by servo electronics and is used to compensate for any environmentally induced noise. A control voltage is fed to the PZT which then moves the reference mirror to create an optical path change that opposes any optical path change resulting from environmental disturbance. In this way, the environmental noise in the measurement interferometer is compensated for. The reference interferometer will be locked at around quadrature to maximize sensitivity to environmental disturbance. Most normal floor vibration occurs in the range from 20 to 200 Hz [33]. Modern PZTs have a resolution up to 0.05 nm and a frequency response of 35 kHz (e.g., P-249.10, Physik Instrumente, Karlsruhe, Germany), the noise compensation can be quick and accurate provided that the load is light. This technique has been effectively tested and proved in our previous research [34,35].

3. Phase Calculation Principle

Intensities detected by pixels (x,y) of the CCD camera that correspond to one point on the test surface can be expressed by

$$I(x,y;k) = a(x,y;k) + b(x,y;k)\cos(2\pi k h(x,y)), \tag{2}$$

where $a(x,y;k)$ and $b(x,y;k)$ are the background intensity and fringe visibility, respectively; k is the wavenumber, which is the reciprocal of the wavelength; and $h(x,y)$ is the absolute OPD of the interferometer. The phase of interference signal $\varphi(x,y;k)$ is given by

$$\varphi(x,y;k) = 2\pi k h(x,y). \tag{3}$$

The phase shift of the interference signal owing to the wavenumber shift is given by

$$\Delta\varphi(x,y;\Delta k) = 2\pi \Delta k h(x,y). \tag{4}$$

The phase change of the interference signal is proportional to the wavenumber k change. Then the OPD, $h(x,y)$, is given by

$$h(x,y) = \frac{\Delta\varphi(x,y,\Delta k)}{2\pi\Delta k}. \tag{5}$$

Since the change of k can be calibrated first by using an optical spectrum analyzer, the main issue here is how to calculate the phase change. There are many phase calculation methods that can be

employed in spectral scanning interferometry. These algorithms include phase demodulation by a lock-in amplifier [36], phase calculation by a seven-point method used in classical phase-shifting interferometry [28], extremum position counting [27], and Fourier transform based techniques [37]. We use phase calculation by Fourier transform because it is fast, accurate, and insensitive to intensity noise.

In Eq. (2), as mentioned, $a(x,y;k)$ and $b(x,y;k)$ are slowly variable with respect to k because of the spectrum intensity of the light source and the response of the CCD camera. The path difference of the interferometer is adjusted to be large enough so that the frequency of the cosine term is higher than the variation frequency of $a(x,y;k)$ and $b(x,y;k)$ so that they can be easily separated from each other. Equation (2) can be rewritten as

$$I(x,y;k) = a(x,y;k) + \frac{1}{2}b(x,y;k)\exp[2\pi ikh(x,y)] + \frac{1}{2}b(x,y;k)\exp[-2\pi ikh(x,y)]. \quad (6)$$

The Fourier transform of Eq. (6) with respect to k can then be written as

$$\hat{I}(x,y;\xi) = A(x,y;\xi) + B(x,y;\xi - h(x,y)) + B(x,y;\xi + h(xy)), \quad (7)$$

where the uppercase letters denote the Fourier spectra of the signal expressed by the corresponding lowercase letters. If $h(x,y)$ were chosen to be higher than the variation of $a(x,y;k)$ and $b(x,y;k)$, the three spectra could be separated from one another. To retrieve the phase distribution of the fringe, the term $B(x,y;\xi - h(x,y))$ is selected and thus the background intensities $a(x,y;k)$ are filtered out. The inverse fast Fourier transform (IFFT) of $B(x,y;\xi - h(x,y))$ is

$$\mathrm{IFFT}(B(x,y;\xi - h(x,y))) = \frac{1}{2}b(x,y;k)\exp[ikh(x,y)]. \quad (8)$$

Taking the natural logarithm of this signal yields

$$\log\left\{\frac{1}{2}b(x,y;k)\exp[2\pi ikh(x,y)]\right\} = \log\left[\frac{1}{2}b(x,y;k)\right] + i\varphi(x,y;k) \quad (9)$$

from which the imaginary part is precisely the phase distribution to be measured. Following the above procedures, the phase distribution of each CCD pixel and the height map of the surface to be measured can be acquired. Since the main operation here is FFT and IFFT, the data processing is fairly fast.

4. Measurements and Results

The method described in Section 3 was used to measure two step height standard specimens. In the experiment, the radio frequency applied to the AOTF (Model LSGDN-1, SIPAT Company, Chongqing, China) was scanned from 80 to 110 MHz in steps of 10 kHz, corresponding to a wavelength interval of 0.48 nm. This radio frequency range provides a scanning wavelength range of from 680.8 to 529.4 nm. During the wavelength scanning process, 300 interferograms were recorded by a high speed CCD camera (Model OK-AM1131, JoinHope Image Technology, Beijing, China) at a rate of 100 frames/s. Figure 2(a) shows the intensity distribution recorded by one of the CCD pixels; Fig. 2(b) shows the corresponding retrieved phase of this intensity distribution, as determined by the data processing

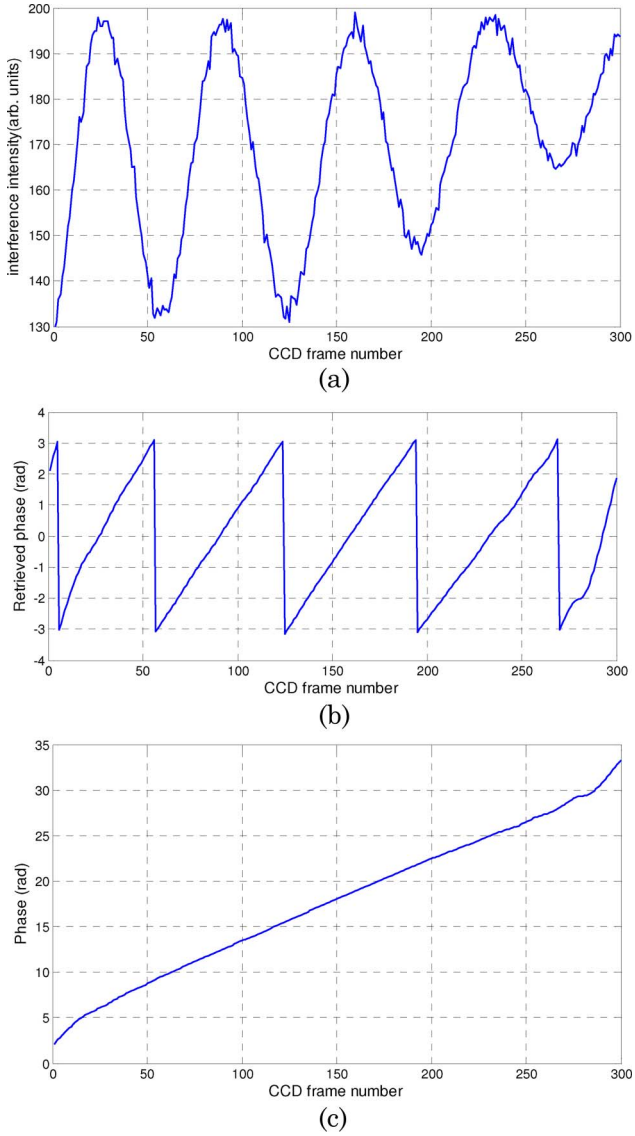

Fig. 2. (Color online) Measured interference fringe and retrieved phase distribution: (a) intensity distribution for 300 interferograms captured by CCD pixels (100, 100), (b) retrieved phase discontinuities distribution, (c) phase continuity distribution.

procedure described by Eqs. (7)–(9). Figure 2(b) suffers from discontinuities, that is, the values are in the range from $-\pi$ to π. These discontinuities were corrected by adding 2π at the discontinuous points to obtain continuous phase distribution as shown in Fig. 2(c). Finally, by using the continuous phase distribution and Eq. (5), the surface height can be calculated for that pixel.

Two experiments were carried out. Figure 3 is a 2.970 μm step height standard as supplied by the National Physical Laboratory (NPL), UK. This sample was processed according to the above proposed measurement procedure and an areal surface view was obtained as shown in Fig. 3(a). Figure 3(b) shows a cross-sectional view of the grooves. The measured average step height is 2.971 μm; the measurement error is 1 nm. All the calculations on step height are calculated according to ISO standard 5436-1 using Talymap as supplied by Taylor-Hobson. Leicester, UK.

Figure 4 shows a 292 nm step height standard specimen that was calibrated by Physikalisch-Technische Bundesanstalt. The areal surface measurement result of this sample is shown in Fig. 4(a). Figure 4(b) illustrates the cross-sectional plot of the step. The measured average step height is 291.1 nm; the measurement error is 0.9 nm.

The effectiveness of the vibration compensation was investigated by carrying out the following experiments. First, a semiconductor daughterboard sample was measured without inducing mechanical disturbance as shown in Fig. 5(a). One profile of the sample is shown in Fig. 5(b) and illustrates the surface step with height 4.7564 μm. Next, a 40 Hz and 400 nm peak-to-peak sinusoidal mechanical disturbance

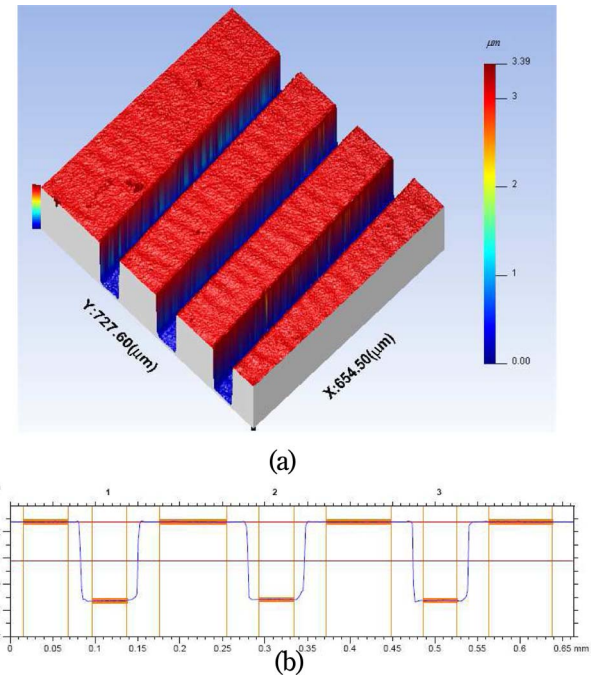

Fig. 3. (Color online) Measurement results of a 2.97 μm standard step: (a) measured surface and (b) cross-sectional profile.

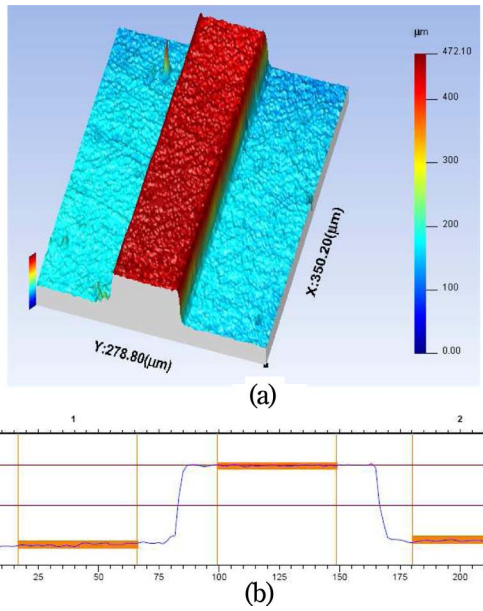

Fig. 4. (Color online) Measurement results of a 292 nm step height standard: (a) measured surface and (b) cross-sectional profile.

using a PZT was applied to the reference mirror. During the disturbance, the sample was measured as shown in Fig. 6. Figure 6(a) shows that the measured signals are suppressed by the mechanical vibration signal, although the step height of the sample can still be recognized. One profile of the sample is shown in Fig. 6(b) and illustrates the surface step with height 11.711 μm. However, the surface roughness signal is completely distorted.

When the vibration compensation is switched on, a reduction in the disturbance movement of the fringe

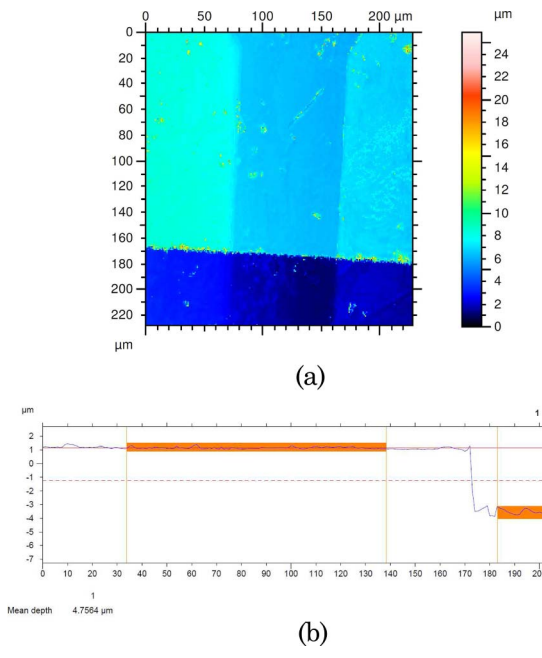

Fig. 5. (Color online) Measurement results of a semiconductor daughterboard sample without an induced mechanical disturbance: (a) measured surface and (b) cross-sectional profile.

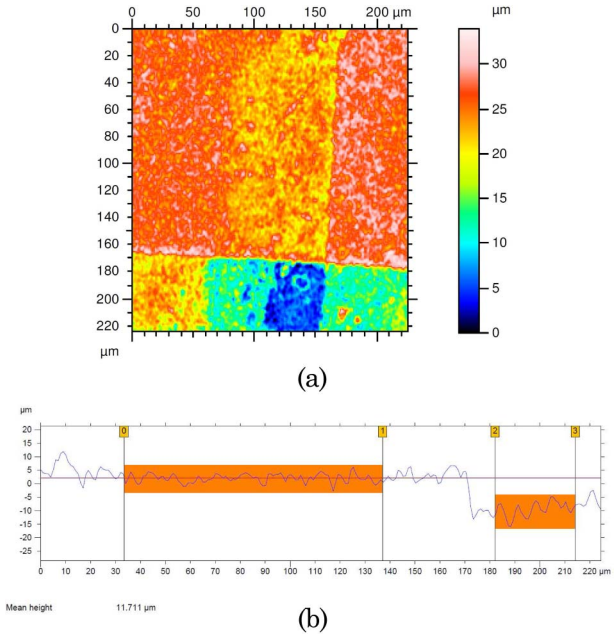

Fig. 6. (Color online) Measurement results of a semiconductor daughterboard sample with a sinusoidal mechanical disturbance of 40 Hz: (a) measured surface and (b) cross-sectional profile.

pattern is clearly observed. The measurement of the sample at this stage is carried out; see Fig. 7. Figure 7(a) shows that the data were retrieved as the original measurement and illustrates that the compensation vibration can be used to overcome environmental disturbance. One profile of the sample cross-sectional plot in Fig. 7(b) shows that the step height is 4.7429 μm. The difference between the two measured step height values is 13.5 nm in comparison with the two measured results as shown in Figs. 5(b) and 7(b). The observed disturbance attenuation between the second and the third parts of the experiment was 12.2 dB according to the reference interferometer signal output as shown in Fig. 8, which is in agreement with the measured sample error.

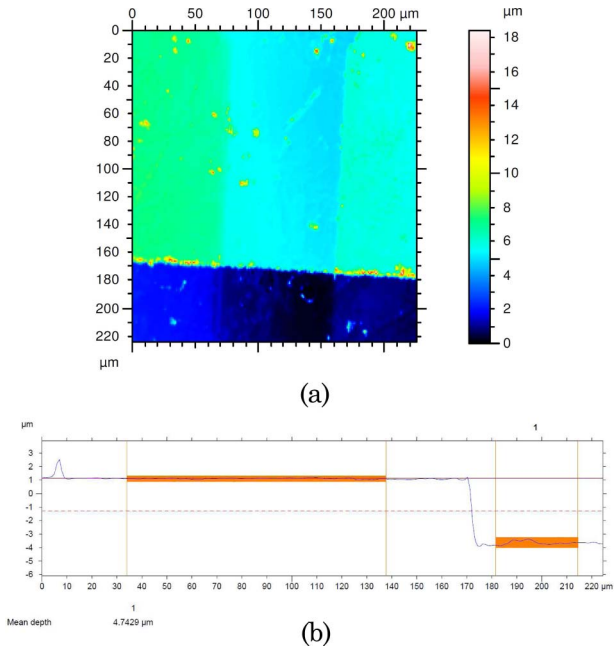

Fig. 7. (Color online) Measurement results of a semiconductor daughterboard sample with vibration compensation: (a) measured surface and (b) cross-sectional profile.

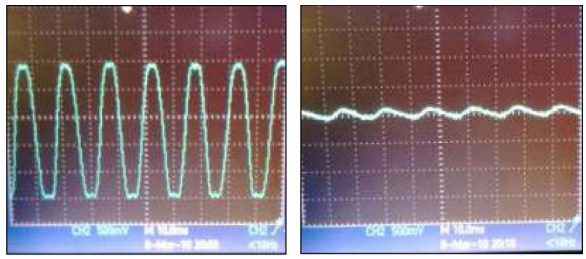

Fig. 8. (Color online) Effect of vibration compensation on a 40 Hz and 400 nm peak-to-peak sinusoidal disturbance: (a) before stabilization and (b) after stabilization.

5. Conclusion

We have proposed a surface measurement technique with active control of environmental noise that utilizes wavelength scanning interferometery. Nanometer accuracy surface measurement results were carried out for micrometer step height samples. There is no need for optical path (mechanical) scanning as found in conventional white-light vertical scanning interferometery. An 850 nm wavelength laser diode shares the same optical path of the measurement interferometer to introduce a vibration compensation feedback loop. The experiment shows that disturbance was reduced by 12.2 dB at a vibration frequency of 40 Hz.

The measurement speed is restricted only by the frame rate of the CCD camera and the data processing speed. A CCD with a higher frame rate could reduce the data acquisition time to less than 1 s. In contrast, the data processing speed for 320 × 320 pixels takes 9 s when calculated with an Intel Pentium D945 processor. It is not ideally fast since general CPUs do not support parallel computing. Stream computing based on GPU parallelization techniques is currently under investigation and could significantly improve the data processing speed by as much as 100 times at an affordable price. Fast areal surface measurement results will be available at high speed when this computing algorithm is realized during the next stage of research.

Xiangqian Jiang gratefully acknowledges the Royal Society under a Wolfson-Royal Society Research Merit Award and the European Research Council under its programme ERC-2008-AdG 228117-Surfund. The authors gratefully acknowledge the Integrated Knowledge Centre (IKC) of the Engineering and Physical Sciences Research Council (EPSRC), UK, for supporting this research. We also thank W. Zeng and H. Martin for fruitful discussions.

References

1. K. W. Lyons, "Integration, interoperability, and information management:whatarethekeyissuesfornano-manufacturing?," Proc. SPIE **6648**, 66480D (2007).
2. A. Siegel and G. Liftin, "Deutsche Agenda Optische Technologien fur das 21 Jarhundert, Lenkungskreis Optische Technologien fur des 21 Jarhundert" (2000).
3. W. B. Lee, "Market trends and applications of ultra-precision freeform machining technology," presented at the Workshop on Design and Fabrication of Freeform Optics for Photonics and Telecommunication Industries, Hong Kong, March 2005.
4. H. Heeren and A. El-Fatatry, "Metrology and characterization for micro and nano technology," presented at Design-for-Purpose Metrology Expert Workshop, Loughborough, UK, 19 May 2008.
5. J. E. Millerd, N. J. Brock, J. B. Hayes, and J. C. Wyant, "Instantaneous phase-shift, point-diffraction interferometer," Proc. SPIE **5531** 264–272 (2004).
6. C. Koliopoulos, "Simultaneous phase shift interferometer," Proc. SPIE **1531**, 119–127 (1991).
7. H. Kihm and S. Kim, "Fiber-diffraction interferometer for vibration desensitization," Opt. Lett. **30**, 2059–2061 (2005).
8. B. Ngoi, K. Venkatakrishnan, and N. Sivakumar, "Phase-shifting interferometry immune to vibration," Appl. Opt. **40**, 3211–3214 (2001).
9. M. North-Morris, J. VanDelden, and J. C. Wyant, "Phase-shifting birefringent scatterplate interferometer," Appl. Opt. **41**, 668–677 (2002).
10. J. Huang, T. Honda, N. Ohyama, and J. Tsuiiuchi, "Fringe scanning scatter plate interferometer using a polarized light," Opt. Commun. **68**, 235–238 (1988).
11. D. Su and L. Shyu, "Phase-shifting scatter plate interferometer using a polarization technique," J. Mod. Opt. **38**, 951–959 (1991).
12. G. S. Kino and S. S. C. Chim, "Mirau correlation microscope," Appl. Opt. **29**, 3775–3783 (1990).
13. B. Bowe and V. Toal, "White light interferometric surface profiler," Opt. Eng. **37**, 1796–1799 (1998).
14. A. Hirai, K. Seta, and H. Matsumoto, "White-light interferometry using pseudo random-modulation for high-sensitivity and high-selectivity measurements," Opt. Commun. **162**, 11–15 (1999).
15. T. Dresel, G. Hausler, and H. Venzke, "Three-dimensional sensing of rough surfaces by coherence radar," Appl. Opt. **31**, 919–925 (1992).
16. A. Hirai and H. Matsumoto, "High-sensitivity surface profile measurements by heterodyne white-light interferometer," Opt. Eng. **40**, 387–391 (2001).
17. G. Häusler, P. Ettl, M. Schenk, C. Bohn, and I. Laszlo, "Limits of optical range sensors and how to exploit them," in *International Trends in Optics and Photonics ICO IV*, T. Asakura, ed., Vol. 74 of Springer Series in Optical Sciences (Springer-Verlag, 1999), pp. 328–342.
18. M. Fleischer, R. Windecker, and H. J. Tiziani, "Theoretical limits of scanning white-light interferometry signal evaluation algorithms," Appl. Opt. **40**, 2815–2820 (2001).
19. S. Kuwamura and I. Yamaguchi, "Wavelength scanning profilometry for real-time surface shape measurement microscope," Appl. Opt. **36**, 4473–4482 (1997).
20. A. Yamamoto, C. Kuo, K. Sunouchi, S. Wada, I. Yamaguchi, and H. Tashiro, "Surface shape measurement by wavelength scanning interferometry using an electronically tuned Ti:sapphire laser," Opt. Rev. **8**, 59–63 (2001).
21. A. Yamamoto and I. Yamaguchi, "Surface profilometry by wavelength scanning Fizeau interferometer," Opt. Laser Technol. **32**, 261–266 (2000).
22. A. Yamamoto and I. Yamaguchi, "Profilometry of sloped plane surfaces by wavelength scanning interferometry," Opt. Rev. **9**, 112–121 (2002).
23. I. Yamaguchi, A. Yamamoto, and M. Yano, "Surface topography by wavelength scanning interferometry," Opt. Eng. **39**, 40–46 (2000).
24. D. S. Mehta, S. Saito, H. Hinosugi, M. Takeda, and T. Kurokawa, "Spectral interference Mirau microscope with an acousto-optic tunable filter for three-dimensional surface profilometry," Appl. Opt. **42**, 1296–1305 (2003).
25. K. Hibino, B. F. Oreb, P. S. Fairman, and J. Burke, "Simultaneous measurement of surface shape and variation in optical thickness of a transparent parallel plate in wavelength-scanning Fizeau interferometer," Appl. Opt. **43**, 1241–1249 (2004).
26. T. Anna, S. K. Dubey, C. Shakher, A. Roy, and D. S. Mehta, "Sinosoidal fringe projection system based on compact and non-mechanical scanning low-coherence Michelson interferometer for three-dimensional shape measurement," Opt. Commun. **282**, 1237–1242 (2009).
27. J. Schwider and L. Zhou, "Dispersive interferometric profilometer," Opt. Lett. **19**, 995–997 (1994).
28. P. Sandoz, G. Tribillon, and H. Perrin, "High-resolution profilometry by using phase calculation algorithms for spectroscopic analysis of white-light interferograms," J. Mod. Opt. **43**, 701–708 (1996).
29. U. Schnell, R. Dandliker, and S. Gray, "Dispersive white-light interferometry for absolute distance measurement with dielectric multilayer systems on the target," Opt. Lett. **21**, 528–530 (1996).
30. K. Joo and S. Kim, "Absolute distance measurement by dispersive interferometry using a femtosecond pulse laser," Opt. Express **14**, 5954–5960 (2006).
31. P. Hlubina, "Dispersive white-light spectral interferometry to measure distances and displacements," Opt. Commun. **212**, 65–70 (2002).
32. E. Papastathopoulos, K. Koerner, and W. Osten, "Chromatic confocal spectral interferometry," Appl. Opt. **45**, 8244–8252 (2006).
33. J. Hayes, "Dynamic interferometry handles vibration," Laser Focus World **38**(3), 109–113(2002).
34. H. Martin, K. Wang, and X. Jiang, "Vibration compensating beam scanning interferometer for surface measurement," Appl. Opt. **47**, 888–893 (2008).
35. X. Jiang, K. Wang, and H. Martin, "Near common-path optical fiber interferometer for potentially fast on-line microscale–nanoscale surface measurement," Opt. Lett. **31**, 3603–3605 (2006).
36. X. Dai and S. Katuo, "High-accuracy absolute distance measurement by means of wavelength scanning heterodyne interferometry," Meas. Sci. Technol. **9**, 1031–1035 (1998).
37. M. Takeda and H. Yamamoto, "Fourier-transform speckle profilometry: three-dimensional shape measurements of diffuse objects with large height steps and/or spatially isolated surfaces," Appl. Opt. **33**, 7829–7837 (1994).